Interpreting two-dimensional cuts through broken geologic objects: Fractal and non-fractal size distributions

Allen F. Glazner* and Ryan D. Mills
Department of Geological Sciences, University of North Carolina, Chapel Hill, North Carolina 27599-3315, USA

ABSTRACT

Numerical simulations and physical fragmentation experiments confirm the theoretical prediction that the fractal dimension of a two-dimensional (2-D) cut through a set of three-dimensional objects with fractal dimension *D* is approximately equal to *D* – 1. This leads to a size distribution in two-dimensional cuts that is skewed strongly toward larger objects compared to the three-dimensional distribution. Three-dimensional shape (aspect ratio) does not significantly affect the resulting 2-D size distribution except for highly nonequant objects, such as prolate ellipsoids with aspect ratios of 10 or more. In contrast, fragmentation of an object by breakage along persistent fractures results in a non-fractal distribution of sizes and far fewer small objects than predicted by fractal statistics. Powdering a rock by extensive crushing also results in non-fractal size distributions because particles are reduced to sizes on the order of 1 μm, a comminution limit below which further brittle fracture is difficult. Natural examples of fragmental objects observed in two-dimensional cuts, such as crushed rocks, breccias, and xenoliths, are generally consistent with a three-dimensional fractal dimension near 2.5 over one or two orders of magnitude in size. However, a limestone breccia from Death Valley exhibits a non-fractal size distribution consistent with fragmentation of a strongly jointed rock. Mafic enclaves in Yosemite National Park have a restricted size range of about one order of magnitude and a three-dimensional fractal dimension of ~3.1, consistent with other enclave swarms. The restricted size range of enclaves may reflect the apertures of mafic dikes that fed them.

*Email: afg@unc.edu.

INTRODUCTION

Although geologic objects are three-dimensional (3D), geologists are typically presented with two-dimensional (2D) cuts through them, such as outcrops, road cuts, and thin sections. It is known that such cuts can be misleading; for example, the clasts in a clast-supported conglomerate generally do not appear to touch each other in outcrop because the outcrop surface rarely intersects the points of contact (Boggs, 1992, p. 212–213). Converting 2D analyses to 3D (stereology) is a common practice in crystal size distribution analysis (Chayes, 1950; Higgins, 1994, 2000; Peterson, 1996) and other geologic intersection work (Sahagian and Proussevitch, 1998). The 3D size distribution of clastic material is important because it provides information about the fragmentation processes of the original object.

Three-dimensional analysis of a large variety of materials produced by crushing, blasting, grinding, thermal shock, and other fragmentation processes shows that the resultant particles tend to follow a self-similar (fractal) size distribution (Turcotte, 1986). That is, if particles whose sizes follow a fractal distribution are passed through a sieve and photographed, and the photograph is then scaled so that the largest particles are of a given size, the size distribution in the photograph will look the same regardless of the sieve size. However, dicing a solid by random orthogonal cuts generates a decidedly non-fractal distribution of particle sizes (Glazner and Bartley, 2006). This suggests that size distributions can be useful in determining fragmentation mechanisms. For example, the size distribution of xenoliths in a pluton might be used to infer whether they were incorporated via thermal fragmentation, producing a fractal size distribution, or by a process involving magma injection along preexisting fractures, producing a non-fractal distribution. Similarly, Shimamoto and Nagahama (1992) used fragment size statistics to argue against a fracture origin for the matrix of pseudotachylites. However, such analyses are hindered by the necessity to analyze materials in two dimensions in outcrop or thin section, and the necessity to understand how 2D cuts relate to 3D objects.

A fractal size distribution is defined by

$$N = Cr^{-D}, \quad (1)$$

where N is the number of fragments with linear dimension greater than r, C is a constant, and D is the fractal dimension. In such a distribution, a log-log plot of the cumulative number of particles greater than a given size r versus r gives a straight line whose slope is $-D$. The greater the value of D, the greater the number of smaller particles relative to larger ones; for example, if $D = 3$, then the number of particles larger than X in linear dimension is 1000 times greater than the number of particles larger than $10X$.

Hartmann (1969) summarized data on fragmentation by various processes such as crushing, blasting, grinding, and explosive volcanic eruption, and showed that the data generally fit a power-law distribution. Turcotte (1986) showed that these data are consistent with a fractal distribution. Figure 1 and Table 1 summarize 319 published D values determined for a variety of fragmented geologic materials in both 3D and 2D. The 3D values have an overall mean of 2.2 ± 0.35 (1 standard deviation), or 2.4 ± 0.3 without the values of Perugini et al. (2011), a large data set that is a distinct outlier in Figure 1. Two-dimensional D values from previous studies of broken solids (Fig. 1) are noticeably lower (1. 5 ± 0.4). Allègre et al. (1982), Turcotte (1986), and Sammis et al. (1987) presented a variety of mechanical and mathematical fragmentation processes that produce particle arrays with D in the range of 2.5 to 2.9. In particular, Sammis et al. (1987) developed a model showing that if nearest neighbors of the same size are preferentially broken, as is commonly found in

Geosphere; August 2012; v. 8; no. 4; p. 902–914; doi:10.1130/GES00731.1; 18 fi gures;1table.
Received 17 June 2011 Revision received 22 April 2012 Accepted 23 April 2012 Published online 26 June 2012

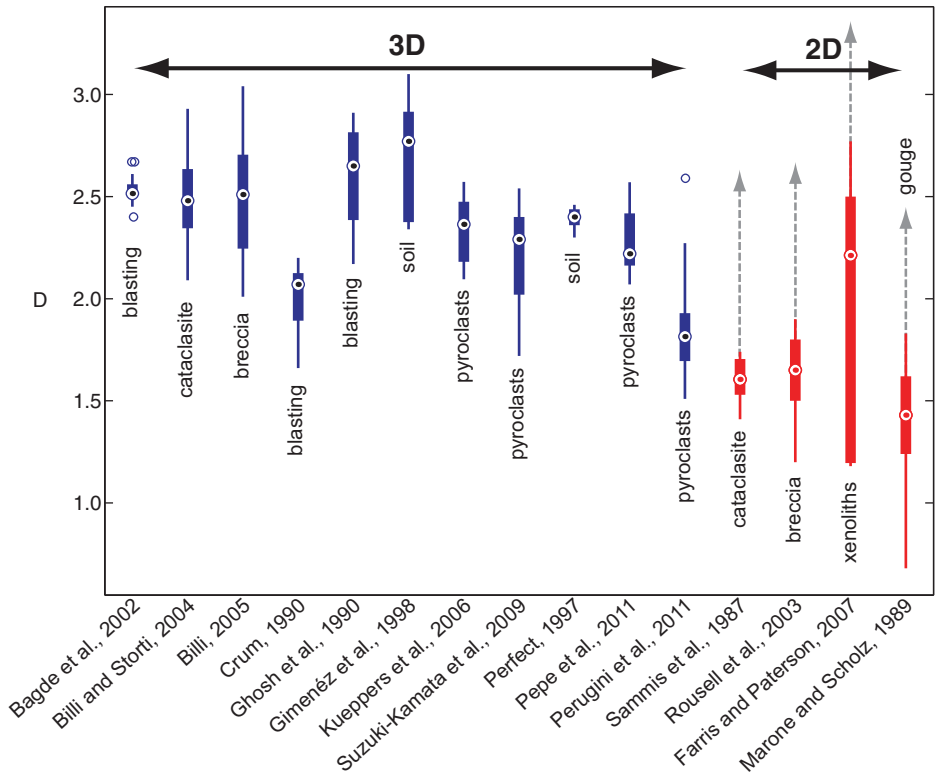

Figure 1. Box and whisker plots of 307 fractal coefficients determined for a variety of fragmented geologic materials in 3D and 2D, including pyroclasts, cataclasites, soils, breccias, and mine blast products. The 3D values have an overall mean of 2.2 ± 0.7 (2 standard deviations), or 2.4 ± 0.6, if the values of Perugini et al. (2011) are eliminated. For each data set, the open circle with a dot is the median, the heavy bar gives the 25th and 75th percentiles, the light line gives the range, and open circles are statistical outliers. Gray arrows for 2D data sets give the median value +1. The Perugini data set is characterized by much lower *D* values than those from other studies, perhaps owing to fragility of the pyroclasts. Data from cataclasite and fault gouge (Sammis et al., 1987; Marone and Scholz, 1989; Billi and Storti, 2004; Billi, 2005); impact breccia (Rousell et al., 2003); pyroclasts (Kueppers et al., 2006; Perugini et al., 2007; Pepe et al., 2008; Suzuki-Kamata et al., 2009; Perugini et al., 2011); soil (Perfect, 1997; Gimenéz et al., 1998); xenoliths (Farris and Paterson, 2007); and mine blasting (Crum, 1990; Ghosh et al., 1990; Bagde et al., 2002).

experiments, then any initial distribution of particles will tend toward a self-similar distribution having a fractal dimension of 2.58.

An alternative description of fragmentation statistics is the lognormal distribution (Hatch and Choate, 1929), which is commonly applied in studies of sedimentary particles (Krumbein and Tisdel, 1940; Folk and Ward, 1957; Rogers, 1965). Hartmann (1969) suggested that the discrepancy between lognormal and power-law fits is in part due to limitations of observational methods, which must always undercount the smallest particles. Some studies have shown that fragmentation processes can produce fragments that are best described as either mixed lognormal–power law or two–power-law populations (e.g., Meibom and Balslev, 1996; Tavassoli and Shirvani, 2000; Yazdi and Esmaeilnia, 2009).

If a fractal array of particles is viewed in a 2D cut, the fractal dimension of the intersected particles, hereafter referred to as D_2, is less than the fractal dimension of the 3D particles, hereafter D_3. Mandelbrot (1983) proposed that when an n-dimensional set of particles with fractal dimension D_n is cut by an n-1-dimensional surface, the fractal dimension of the particles viewed in that surface should be $D_n - 1$ provided that the particles are isotropic in the missing dimension. Thus, an array of particles with $D_3 = 2.5$ cut by a planar surface should have $D_2 = 1.5$. This conjecture has been discussed by Sammis et al. (1987), Russ (1994, p. 301ff), and Tang and Marangoni (2006), among others.

An intuitive explanation of Mandelbrot's conjecture is shown in Figure 2. In a random cut through a series of spheres of differing diameters, larger spheres are more likely to be intersected than smaller ones. In particular, a sphere of radius R is 10 times more likely to be intersected than one of radius $R/10$. Thus, every decrease in size of a factor of 10 leads to a tenfold decrease in the probability that a particular particle will be counted, decreasing the slope of the fractal plot by one.

In this paper, we examine the size distributions of 3D particles in 2D cuts using numerical simulations and experimental studies, and compare them to outcrop data from breccias and xenoliths.

NUMERICAL SIMULATIONS

Data to be fit by Equation 1 are generally grouped into size classes and then displayed on a plot of log(N) versus log(r) (e.g., Turcotte, 1986). We use a slightly different but equivalent technique in which the length observations are ranked from largest to smallest and then plotted against s – 1, where s is the rank. This method has the advantages of eliminating the arbitrariness of histogram binning and more clearly showing the effects of left-hand and right-hand truncation (see below).

We generated fractally distributed (in edge length or diameter) populations of 3D objects (cubes, tetragonal prisms, spheres, and tetrahedra) with $D = 2.5$ using inverse transform sampling (Devroye, 1986, Chap. 2). If F is the cumulative distribution function of a given probability distribution, then inserting uniform random numbers drawn from the interval [0,1] (U[0,1]) into the inverse function F^{-1} yields random numbers drawn from the probability distribution described by F. The fractal distribution of Equation 1 is itself a cumulative probability distribution.

The general algorithm for the simulations is as follows:

(1) Generate a vector r of fractally distributed lengths by inserting a vector of n random numbers drawn from U[0,1] into the function $x^{-1/2.5}$.

(2) Generate a vector z of n random numbers drawn from U[0,100], and distribute the n objects along the z-axis using these numbers.

(3) Calculate the cross-sectional area of the objects cut by the plane $z = 50$.

Following Turcotte (1986), we use the square root of the area (referred to below as eigenlength) as a linear measure of the object's size, both in simulations and with natural data. Calculations were done in Matlab. With this algorithm, the minimum value of r approaches 1. Thus, in Equation 1, $C = n - 1$. The simulations are insensitive to the size of the interval drawn from (e.g., [0,100]) provided that it is large compared to the objects being studied.

TABLE 1. COMPILATION OF 3D AND 2D FRACTAL DIMENSIONS

Source	Material	D_3	D_2	s.d.*
Literature values				
Bagde et al. (2002)	Mine blasting	2.53		0.08
Billi and Storti (2004)	Carbonate cataclasite	2.49		0.21
Billi (2005)	Limestone breccia	2.50		0.30
Crum (1990)	Mine blasting	2.00		0.16
Ghosh et al. (1990)	Mine blasting	2.61		0.24
Gimenéz et al. (1998)	Soil	2.69		0.28
Kueppers et al. (2006)	Pyroclasts (experimental)	2.34		0.15
Suzuki-Kamata et al. (2009)	Pyroclasts	2.22		0.25
Perfect (1997)	Soil	2.39		0.06
Pepe et al. (2008)	Pyroclasts	2.29		0.16
Perugini et al. (2011)	Pyroclasts	1.83		0.18
Glazner and Bartley (2006)	Granite (thermal disaggregate)	2.20		n.d.†
Sammis et al. (1987)	Gneiss cataclasite		1.60	0.12
Rousell et al. (2003)	Impact breccia		1.62	0.26
Holtz et al. (1987)	Enclaves		1.82	0.19
Perugini et al. (2007)	Enclaves		2.50	n.r.§
Farris and Paterson (2007)	Xenoliths		2.00	0.75
Marone and Scholz (1989)	Fault gouge (experimental)		1.39	0.29
This study (all D_3 = 2.5)				
Numerical	Oriented cubes		1.50	
	Random cubes		1.62	
	Spheres		1.52	
	Oriented tetrahedra		1.55	
	Random ellipsoids, k = 0.1		1.58	
	Random ellipsoids, k = 5		1.51	
	Random ellipsoids, k = 10		1.69	
	Random ellipsoids, k = 20		1.91	
Physical	Rhyolite	2.51	1.49	
	Granite	2.37	n.d.	
	Calcite		Nonlinear#	
	Fluorite		Nonlinear#	
	Amphibole		2.00*	
	Xenoliths in granodiorite		1.44	
	Granodiorite fault breccia		1.87	
	Limestone breccia		Nonlinear#	
	Mafic enclaves in granodiorite		2.20	

*One standard deviation of measurements.
†Not determined.
§Not reported.
#Curved size distribution, not self-similar.

Figure 3 shows the results of one simulation. One million cubes with fractally distributed edge lengths were placed with a face parallel to the *x-y* plane. Thus, if a given cube is intersected by the plane $z = 50$, the cross-sectional area of the intersection is equal to the full area of a face. The blue curve gives the distribution of edge lengths for the 3D objects, and the red curve for the intersection simulation. The intercept at $r = 1$ for the 3D objects is 10^6, since all 10^6 objects were counted, whereas the corresponding intercept for the 2D intersections is ~16,500, indicating that <2% were cut by the plane. Linear fits to these arrays have calculated slopes of –2.5 and –1.5, verifying that the generating algorithm is correct and that the Mandelbrot (1983) conjecture works for this system. If the cubes are randomly oriented (green curve), then the calculated fractal dimension is somewhat higher (1.62 in the simulation in Fig. 3) owing to a higher number of small objects that correspond to triangular and rectangular cuts far from the cube center. This value is ~8% higher than that predicted from the $D - 1$ rule.

Spheres and tetrahedra present slightly different cases (Fig. 4). The linear portion of the 2D sphere curve in Figure 4 has a slope of –1.52, but there is a fl at tail at low radii caused by spheres that were intersected far from their equators by the intersection plane. The tetrahedron simulation in Figure 4 consisted of 10^6 regular tetrahedra oriented with a face parallel to the *x-y* plane. The 2D intersection curve for the tetrahedra also has a linear section with a flat left-hand tail; the linear portion has a slope of –1.55 owing to the bias toward small intersection areas toward the apex. For both of these objects, the $D_3 - 1$ method is approximately correct.

Figure 5 shows the size distributions of 2D cuts through randomly oriented ellipsoids of varying aspect ratio, both prolate and oblate. For each curve, 10^5 ellipsoids were generated with fractally distributed equatorial axis a and rotational axis $c = ka$, where k is the aspect ratio. For $k = 1$, the ellipsoids are spheres, and this simulation gives $D_2 = 1.50$ as expected. For $k = 5$, the calculated slope is only slightly different from –1.5, but for $k = 10$ (cigar-like), it is substantially different (–1.69), and for $k = 20$ (pencil-like), it is even higher (–1.9). For highly oblate ellipsoids with $k = 0.1$, the calculated D_2 (–1.58) is again slightly greater than 1.5.

SAMPLING OF FRACTAL DISTRIBUTIONS AND THE TRUNCATION PROBLEM

Measurement of objects drawn from a population with a fractal distribution is confounded by problems of truncation (Pickering et al., 1995). Left-hand (small-scale) truncation is related to the sensitivity of the measurement process; small objects are increasingly difficult to detect as their size decreases. Right-hand (large-scale) truncation occurs under several circumstances. For example, the maximum xenolith area that can be measured in a given exposure cannot exceed the area of the outcrop, and large objects that intersect the edge of the measurement area (such as the edge of a frame undergoing image analysis) are either omitted from analysis (as in this study), or their size is underestimated. If the larger values of a distribution are not sampled, then an array of particles that should plot as a straight line on a fractal plot will instead be convex up, falling below the nominal slope on the right and leading to an overestimate of the fractal dimension (Fig. 6; Pickering et al., 1995).

DATA FROM PHYSICAL EXPERIMENTS

Crushed Rocks and Minerals

As noted earlier, fragmented materials commonly have D ~2.4 ± 0.3 in three dimensions (Fig. 1). Figure 7 shows data from an aphyric, indurated Miocene rhyolite from the western Mojave Desert that was crushed in a jaw crusher such that the largest particles were on the order of 1 cm. The resulting particles (72 g) were put through a stack of sieves, and the numbers in each size range were estimated using the method described by Glazner and Bartley (2006) with an assumed particle density of 2600 kg/m^3. The data array is linear with a slope of –2.51 (the largest and smallest size classes were discounted to minimize truncation issues). A medium-grained quartz monzonite from the Eocene Mount Princeton batholith of central Colorado was similarly processed, yielding $D_3 = 2.37$. Thermal fragmentation of granite by Glazner and Bartley (2006) yielded D_3 ~2.2.

To examine a 2D cut through the crushed rhyolite, an aliquot was passed through a sieve with an opening of 1 mm, and then a small random aliquot was scooped up with a spatula and

stirred into UV-curing epoxy (Norland 63) on a glass slide. The epoxy is viscous (~2.5 Pa·s) and hardened rapidly, ensuring negligible particle settling and size fractionation. After hardening, this mount was polished and imaged on a scanning electron microscope using backscattered electrons, a high probe current, and high contrast. This allowed for unambiguous discrimination of the sectioned particles, which were then counted and measured using ImageJ software (http://imagej.nih.gov/ij).

Figure 8 shows that the largest particles have an eigenlength of ~0.5 mm, and the total number counted was ~1200. In the size range between ~0.03 and 0.3 mm, a line with slope –1.49 fits the data well, but the number of smaller particles is far smaller than described by $D_2 = 1.5$. Thus, in this example, although the 3D particle array has eigenlengths described by D_3 ~2.5 over a size range of ~2.5 orders of magnitude, a 2D cut only follows the $D - 1$ rule over approximately one order of magnitude.

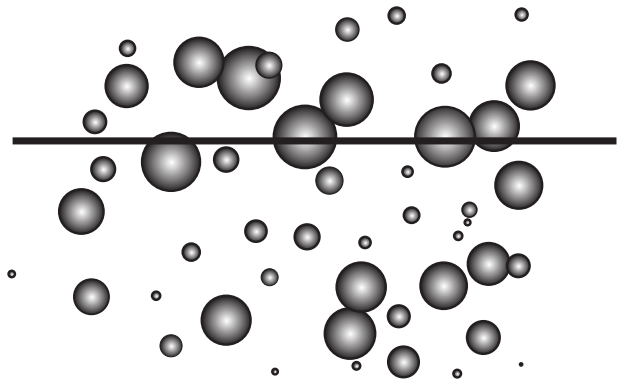

Figure 2. A two-dimensional cut (horizontal line) through a 3D array of objects of variable size will systematically undersample the smaller objects, leading to a small fractal dimension. This is the basis for Mandelbrot's conjecture that if the 3D fractal dimension is *D*, the fractal dimension in a 2D cut will be *D* – 1.

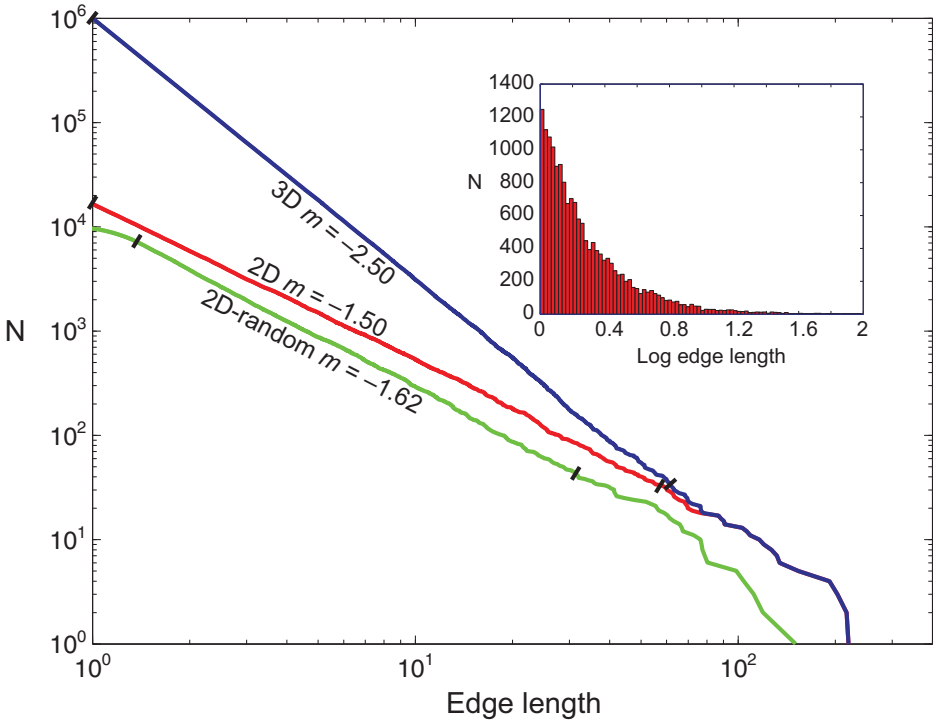

Figure 3. Size distribution for 10^6 cubes generated with a fractal length dimension of 2.5. Blue curve represents the 3D data set; red curve represents the edge length of cubes intersected by a planar cut; and green curve is eigenlength (square root of area) of intersections of randomly oriented cubes with the cut. The slope of the 3D curve is –2.5, consistent with the generating data, and the slope of the 2D curve is –1.5, consistent with Mandelbrot's conjecture. Randomly oriented cubes yield a slightly higher estimate of D_2. Tick marks show segments of curves whose slopes were obtained by least squares. *m*—slope of line segment.

A crushed calcite crystal displays a somewhat different size distribution. A calcite crystal 2 cm in longest dimension was struck lightly with a hammer three times, passed through a 1-mm sieve, and then mounted, imaged, and counted as described above. The resulting data array (Fig. 8B) is noticeably more convex-up than the crushed rhyolite and lacks the central linear segment displayed by the rhyolite particles. It is also noticeably more convex than a lognormal array. Crushed fluorite, another mineral with excellent cleavages, also shows a rounded size distribution (Fig. 8C), whereas crushed amphibole has a short linear segment with a slope of –2.00. The rounded array shapes for calcite and fluorite resemble those produced by dicing a cube by cuts parallel to the three principal face directions. Figure 9 shows 3D and 2D simulations of this process. The 3D simulation follows the method of Glazner and Bartley (2006); for the 2D simulation, rectangular prisms produced by this algorithm were distributed randomly between $z = 0$ and $z = 50$, and areas intersected by a plane at $z = 25$ were determined. Both arrays are continuously curved.

In contrast to the fractal particle array produced when a rock is crushed in a jaw crusher (Fig. 7), rock powder produced by extensive pulverization shows a curved size distribution (Fig. 10). Basalt sample P-36 (Glazner et al., 1991) was crushed in a jaw crusher and then powdered for 10 min in a tungsten carbide ball mill. A small aliquot of powder was shaken vigorously in water, and a small drop of this dilute suspension was placed on a glass slide for analysis under backscattered electrons, yielding full particle diameters. The resulting size distribution is curved and non-fractal (Fig. 10).

Xenoliths and Breccias

In order to look for self-similarity in xenolith size distributions, we collected measurements of 950 xenoliths from the outer margin of the Tuolumne Intrusive Suite in Yosemite National Park, California. Abundant xenoliths occur in the granodiorite of Glen Aulin adjacent to metamorphic wall rocks near the southeastern corner of May Lake. These metamorphic and surrounding igneous rocks were mapped by Rose (1957), Bateman et al. (1983), and

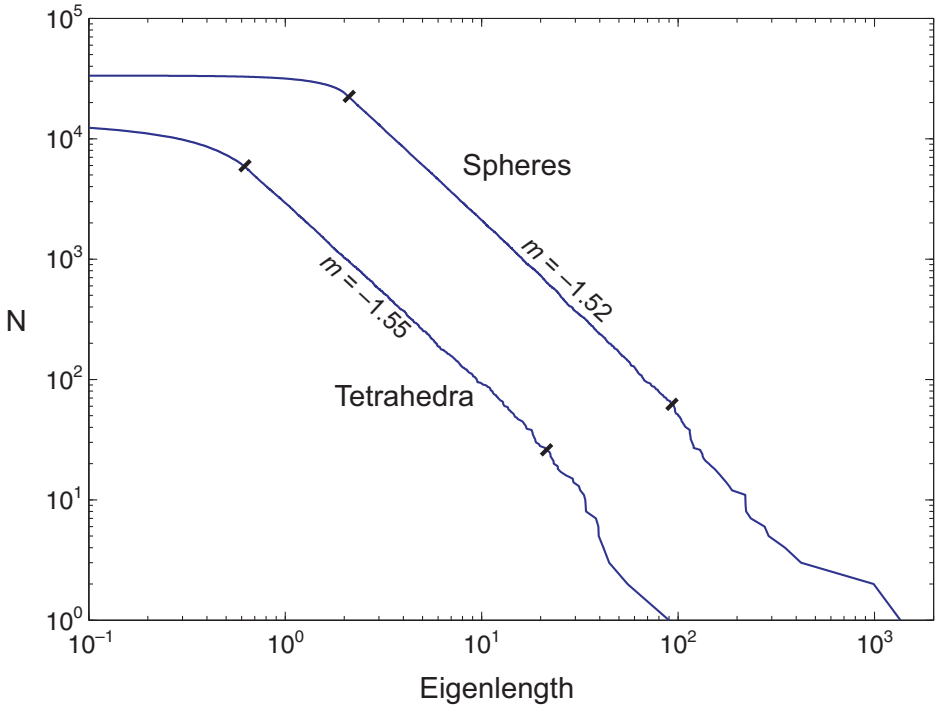

Figure 4. Size distribution of eigenlength (square root of area) of spheres and tetrahedra generated with $D = 2.5$ in 2D cuts. Linear portions of data arrays (between ticks) are slightly steeper, but generally consistent with the $D - 1$ rule. *m*—slope of line segment.

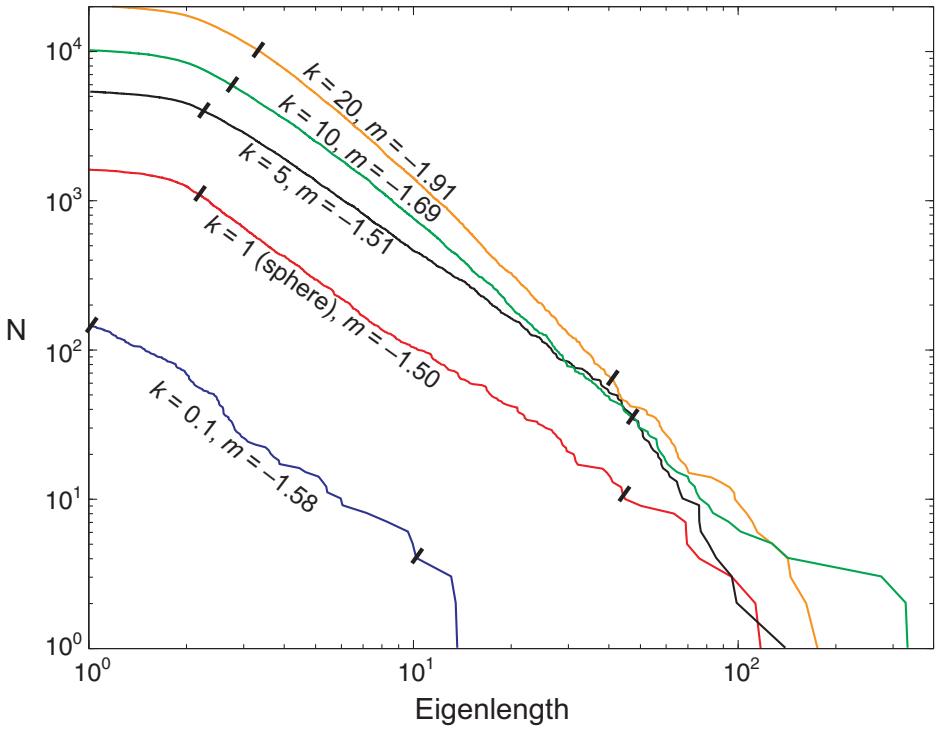

Figure 5. Size distributions of 2D cuts through randomly oriented uniaxial ellipsoids. The parameter *k* is the ratio of the rotational to equatorial axis length for each simulation; for each simulation, *k* was constant, but the axes were fractally distributed. For nonspherical ellipsoids, the calculated fractal coefficient D_2 is greater than 1.5, but the effect is small except for large values of *k*. *m*—slope of line segment.

Taylor (2004), and studied geochemically by Gray et al. (2008) and Mills et al. (2009). As noted by Mills et al. (2009), xenoliths almost exclusively occur where granodiorite is in contact with schistose pelitic quartzite, which is the only foliated rock type in the metamorphic screen, and nearly all measured xenoliths were pelitic quartzite (a few percent were quartzite). Xenoliths with a minor axis length greater than 1 cm were measured in five areas (average area of 50 m^2) with abundant xenoliths and near-100% exposure. Eigenlength was calculated for each xenolith as the geometric mean of the long and short axes.

Figure 11 shows the size distribution of these eigenlengths. A line with a slope of –1.44 fits the data well over a size range from 30 cm to ~4 cm. This indicates that over the relatively restricted size range measured, these xenoliths likely have D_3 ~2.4, consistent with the fragmentation studies summarized in Figure 1. The largest xenolith measured in this study was 1 m^2 in area, although xenoliths over 100 m long occur in the contact zone (Taylor, 2004; Glazner et al., 2004).

We determined D_2 from a photograph of a brecciated fault surface (Fig. 12) and found a somewhat higher fractal dimension. The brecciated surface is from the Castle Mine fault in the Marble Mountains, Mojave Desert, California, a steeply dipping, curved normal fault that places early Miocene rhyolite on Jurassic granodiorite (Glazner and Bartley, 1990). It exhibits abundant polished fault surfaces with steep slickenlines, and brecciated particles are clearly evident on the fault surfaces (Fig. 12). Outlines of particles down to ~0.5 mm across were traced and the resulting array analyzed as above with ImageJ. The size-distribution array (Fig. 13) has a pronounced linear section from ~7 mm to 1 mm, with a slope of –1.87. The magnitude of the slope indicates that there are a greater number of small particles in each successively smaller size class than predicted if the D_3 were 2.5.

Fragments from a limestone breccia in Death Valley National Park, California, exhibit a particle size distribution in 2D that differs from both May Lake xenoliths and the Castle Mine fault breccia. This breccia (Fig. 14) occurs in lower Titus Canyon in limestone of the Cambrian Bonanza King Formation (Norris, 1985). The breccia likely formed by cave collapse based on upward termination of the deposit with no apparent relationship to faults in the range, and concentrically zoned calcite layers that fill voids and are probably speleothems (B.P. Wernicke, 2011, personal commun.). The data array from this breccia (Fig. 15) is conspicuously curved.

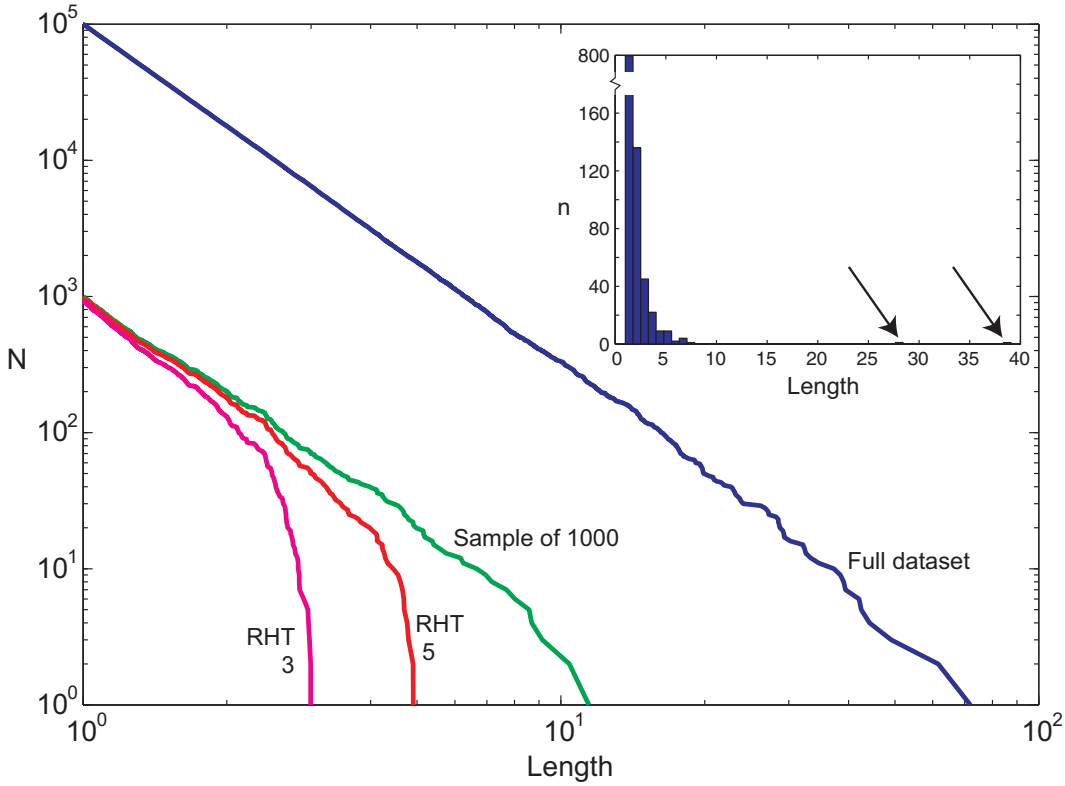

Figure 6. Size-distribution plot showing effects of right-hand truncation (RHT) on curve shape. Blue curve represents 100,000 numbers generated with D = 2.5, and has a slope of –2.5. Inset shows a linear histogram of these values; although most of the data are in the smallest bar (note scale change), a few points are >5, with single values near 28 and 39 (arrows). Green curve is a random sample of 1000 of these points; it too has a slope of –2.5 but is shifted down two orders of magnitude. Red curve represents a subset of these points, with values >5 excluded, and magenta is a subset with values >3 excluded. Note characteristic RHT fall-off below nominal slope of –2.5. Significant RHT causes the slope of the linear portion of the curve to be overestimated (Pickering et al., 1995).

Mafic Magmatic Enclaves

We measured long and short axes of 460 enclaves in a 500 m^2 area of 100% glacially polished exposure in the Half Dome Granodiorite near Tenaya Lake, Yosemite National Park. All enclaves with a minor axis length of at least 1 cm were measured. The largest enclave measured was 70 × 38 cm in dimension, and the geometric mean of their aspect ratios is 2.4. The data array (Fig. 16) displays a linear section that covers approximately one order of magnitude with a slope yielding D_2 ~2.1.

DISCUSSION

Validity of the Mandelbrot Conjecture

The numerical simulations with simple geometric objects described above support the Mandelbrot conjecture that if a 3D set of objects with fractal length dimension D_3 is cut by a 2D plane, D_2 of the intersected objects will be approximately D_3 – 1 for most geologic objects other

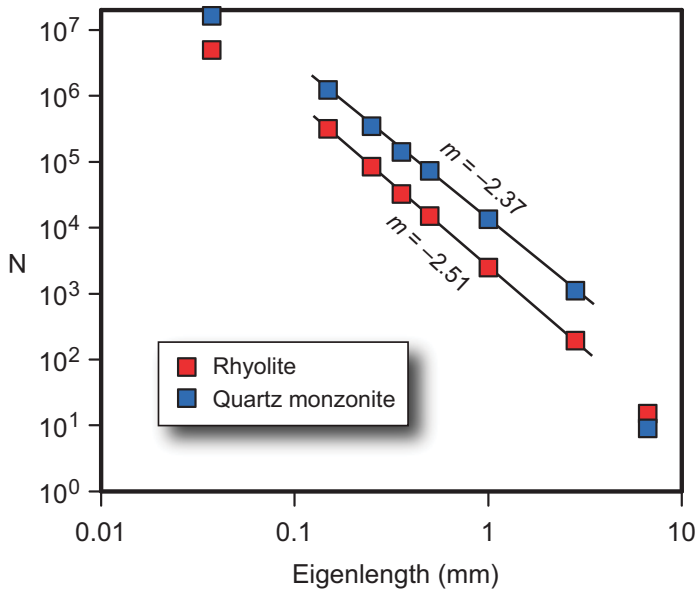

Figure 7. Size-distribution plot for an aphyric rhyolite and a quartz monzonite crushed in a jaw crusher; particle numbers estimated using the method of Glazner and Bartley (2006). The lines have slopes of –2.4 and –2.5, indicating that these particles fit a fractal distribution with D_3 ~2.5 well. *m*—slope of line segment.

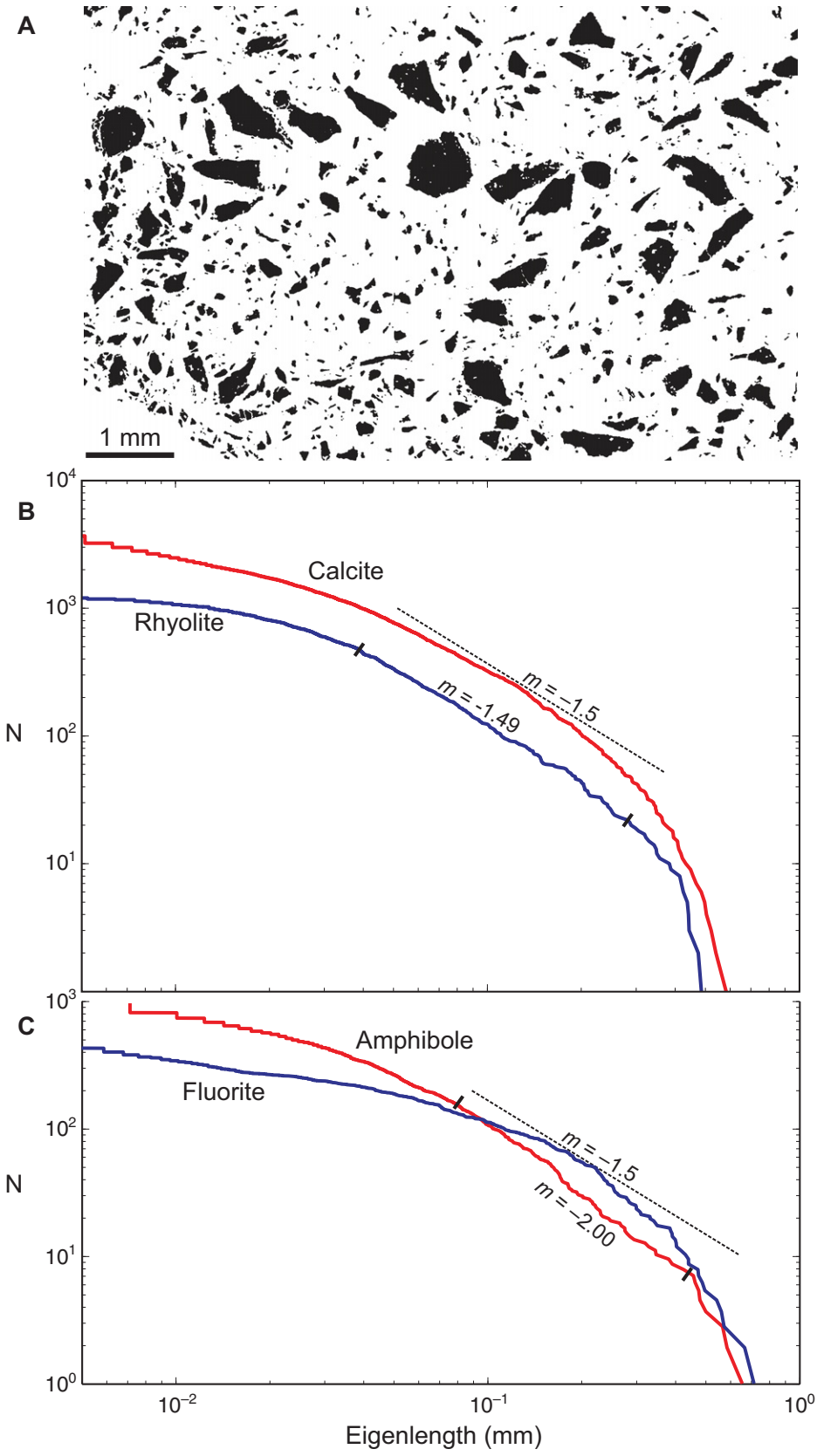

Figure 8. Size-distribution plots for the crushed rhyolite of Figure 7 and for a crushed calcite crystal. (A) Mosaic of backscattered electron images of rhyolite particles mounted in epoxy. This mosaic, and a similar one prepared from the crushed calcite, were analyzed for particle areas. (B) The crushed rhyolite follows the $D - 1$ rule over an order of magnitude, whereas the crushed calcite has no linear section. (C) Crushed amphibole and fluorite. Fluorite shows a curved array similar to calcite; amphibole has a short linear section. *m*—slope of line segment.

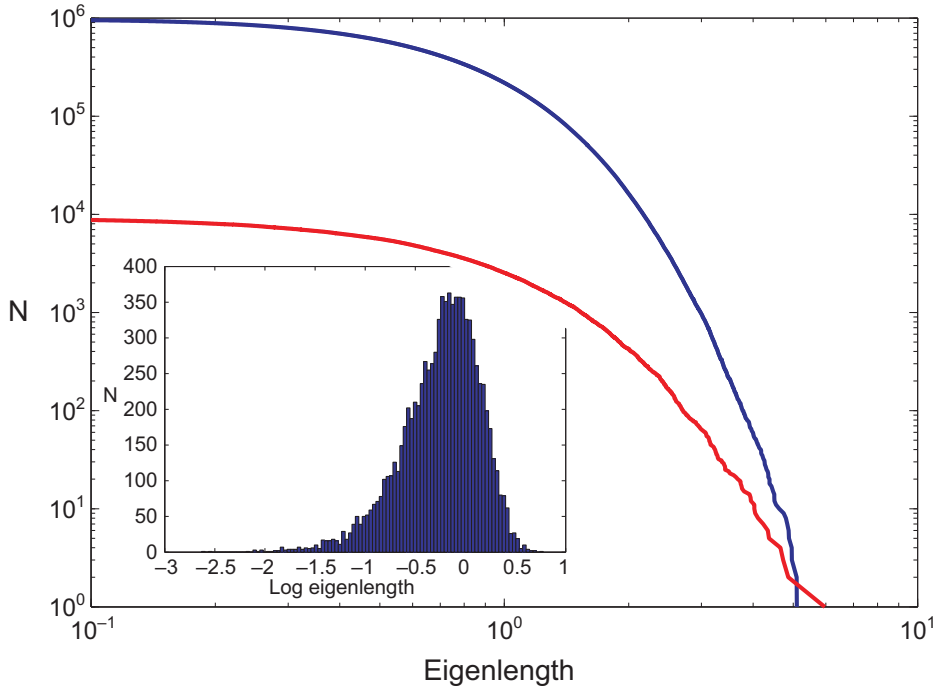

Figure 9. Size-distribution plots for prisms produced by dicing a cube into 10^6 pieces. See text for discussion. Both the 3D array (blue) and 2D section (red) produce strongly curved arrays without linear sections.

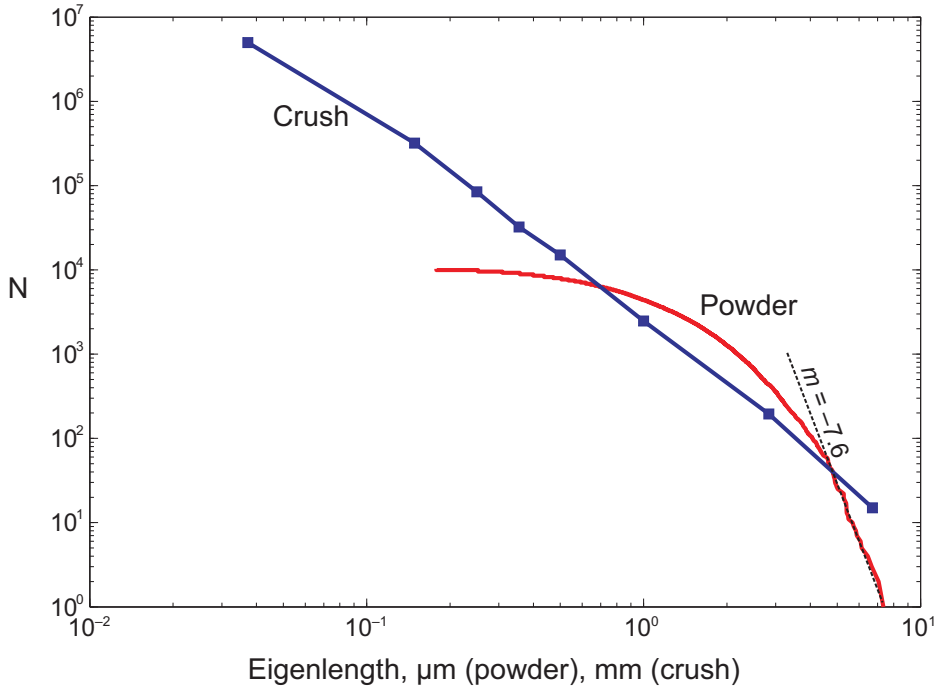

Figure 10. Comparison of self-similar size distribution (crush) of rhyolite produced by crushing rock in a jaw crusher (Fig. 7) with the non–self-similar array (powder) produced by extensive powdering in a ball mill. The linear portion of the powder array is much steeper than the corresponding fractal array generated by crushing, probably due to a comminution limit that governs how finely a rock can be crushed. *m*—slope of line segment.

than those that are highly prolate or oblate. Tang and Marangoni (2006) came to a similar conclusion in a numerical and experimental study of 2D sections through networks of crystalline fat.

Geologic Objects

Geologic objects studied in 2D present a more complicated picture. A crushed rhyolite with a 3D size distribution (Fig. 7) that is best fit by a fractal dimension of ~2.5, when viewed in a 2D section, shows the predicted fractal distribution with D ~1.5 over a limited size range of approximately one order of magnitude (Fig. 8). The distribution tails off with a substantially smaller number of small particles than predicted by $D_2 = 1.5$, and the largest particles are significantly smaller than predicted.

Xenoliths from the outer margin of the Tuolumne Intrusive Suite in Yosemite National Park yield a D_2 of ~1.44 (Fig. 11). As with the crushed rhyolite, the size-distribution plot is convex upward, tailing off for small particles and exhibiting a maximum particle size smaller than predicted by the linear portion of the curve. This paucity of large xenoliths may be an artifact of the areas chosen for study, which specifically avoided the enormous xenoliths that occur in the area (Taylor, 2004)—another case of right-hand truncation.

The Comminution Limit

Measuring the abundance of small particles is problematic owing to limitations of observation (e.g., the resolution of optical techniques), the possibility that small particles are lost during sample preparation, and the effects of truncation. However, the smaller-than-expected number of small particles may instead be a result of a fundamental change in the mode of failure as the material deforms by ductile rather than brittle deformation mechanisms.

Kendall (1978) and Hagan (1981) showed that the mechanics of crack nucleation and propagation impose a limit to the size of particles that can be produced by breakage. Using fracture toughness and hardness data from Broz et al. (2006) and the relation of Hagan (1981), we calculate this comminution limit for quartz and orthoclase as ~0.5 µm. Full physical data are not available for all materials of interest, but similar fracture toughness values for olivine (deMartin et al., 2004) and basalt (Balme et al., 2004) predict comparable comminution limits. For the extensively powdered basalt in Figure 10, the number of particles tails off dramatically below 1 µm even though the resolution of the images used to measure the particles was on the order of 0.1 µm. This result is consistent

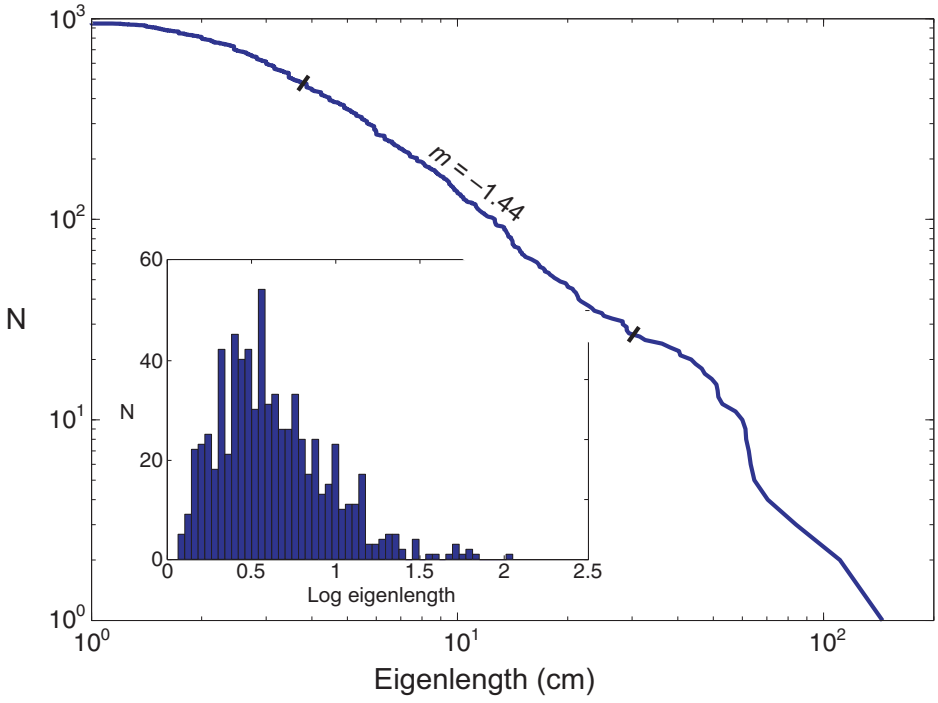

Figure 11. Size-distribution plot for 950 xenoliths at the western contact of the Tuolumne Intrusive Suite near May Lake, Yosemite National Park, California. The main part of the data array exhibits a linear section with D_2 = 1.44, consistent with a fractured 3D array with D_3 = 2.44. *m*—slope of line segment.

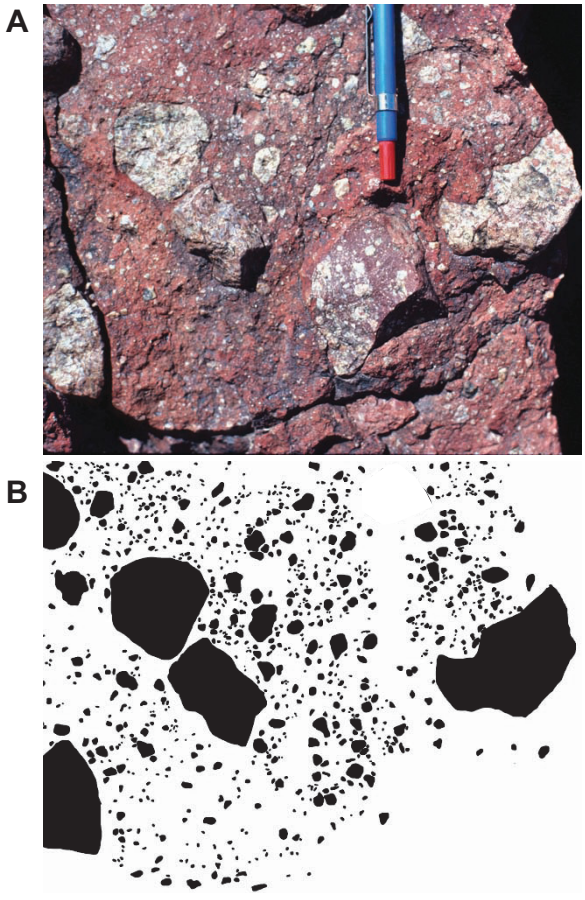

Figure 12. Outcrop photograph of fault breccia (A) and corresponding trace prepared by hand (B) from a fault surface in the Marble Mountains, Mojave Desert, California. Pencil for scale.

with a comminution limit comparable to the calculated value for silicates and with the observation that fine rock powders produced by natural processes, such as glacial flour, commonly have size distributions that dramatically tail off below ~1 µm (Rosenbaum and Reynolds, 2004; however, see Chanudet and Filella, 2008), and with the common observation that powdering of a sample in a ball mill or similar device typically reduces rock fragment size to ~1 µm regardless of how long the process is continued.

We simulated fractal fragmentation of cubes numerically, with and without a lower comminution limit, as follows. One hundred cubes with edge lengths drawn from U[1,100] were generated. At each step, a given cube was fragmented into eight sub-cubes with probability p, and this process was repeated for several steps. When no lower size limit is imposed, a fractal size distribution results (Fig. 17); this is the schematic fragmentation process outlined by Turcotte (1989), and it is insensitive to the starting distribution of edge lengths or number of starting cubes. However, if a lower (comminution) limit is imposed below which a cube will no longer fragment, the size distribution steepens dramatically as larger cubes are fragmented down to this limit.

Dicing versus Fractal Fragmentation

We suggest that the three excellent cleavages of calcite and four of fluorite make their fragmentation process resemble dicing more than the nearest-neighbor crushing process proposed by Sammis et al. (1987). In a true fractal distribution, ever-smaller particles are increasingly abundant, whereas in dicing, ever-smaller particles are less and less likely to be formed because they only form where three pairs of closely placed dicing planes intersect. Thus, throughgoing cleavages may account for the curved data array determined for the crushed calcite and fluorite crystals (Fig. 8). The cleavages allow the crystal to fragment along intersecting fractures and likely signify a fragmentation mechanism that is fundamentally different from fractal fragmentation. Amphibole fragment data in Figure 8 are more difficult to interpret, but the plot does have a short linear section with D_2 = 2.0. With only two good cleavages, amphibole likely exhibits a mix of fragmentation mechanisms.

The Titus Canyon breccia (Figs. 14 and 15) may exhibit a similar distribution due to pervasive fractures that dissect the western margin of the Grapevine Mountains (e.g., Snow et al., 1989). Rather than having been crushed by faulting, this breccia likely formed by collapse, a process that would exploit pervasive fractures. Alternatively, the Titus Canyon breccia may

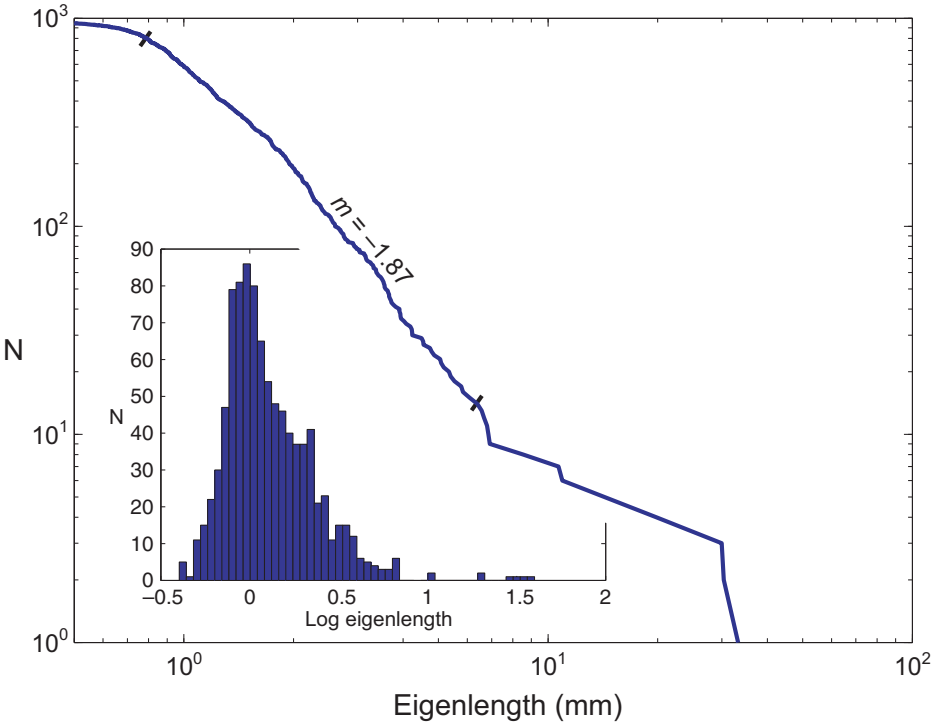

Figure 13. Size-distribution plot for fault breccia fragments measured from the fault surface in Figure 12. This array is difficult to interpret and lacks the fractal behavior of the fault breccias studied by Sammis et al. (1987). *m*—slope of line segment.

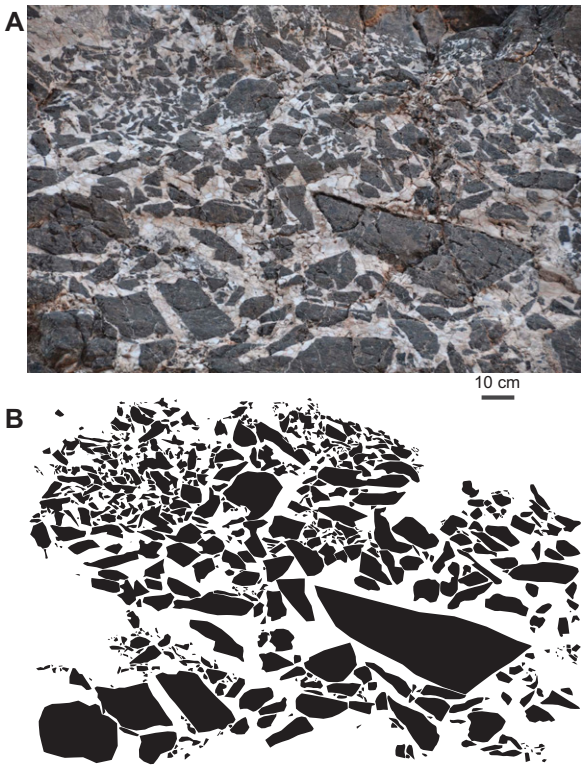

Figure 14. Outcrop photograph of breccia near the mouth of Titus Canyon in Death Valley, California (A) and corresponding trace prepared by hand (B).

have originally had a fractal size distribution with D ~2.5, but after formation small particles were washed out of the system. Water flow through a rubble pile preferentially moves the smaller particles, and such a process could lead to convex-up curvature on an otherwise linear size-distribution plot.

Fragmentation in Igneous Systems

The decrease in fractal dimension caused by viewing particles on cut surfaces has important implications for statistical analysis of such size distributions. Glazner and Bartley (2006) stated that "in a particle group described by a fractal distribution with D = 2.5, for every 10 m block there should be >300 1 m blocks, 100,000 10 cm blocks, and >30,000,000 1 cm blocks. We are unaware that any pluton has been observed to contain millions of small xenoliths for every large one." This reasoning is correct but misleading, because outcrop observations are 2D cuts through these distributions. If D_2 = 1.5, then a relevant restatement would be "for every 10-m block there should be ~32 1-m blocks, >1000 10-cm blocks, and >30,000 1-cm blocks." Data in Figure 11 indicate that the xenolith size distribution near May Lake does reflect a fractal size distribution with D_3 ~2.5 over at least a limited size range.

It is unlikely that we undersampled xenoliths 1–4 cm in eigenlength because measurement was done directly on glacially polished slabs, and xenoliths a centimeter across are easily recognizable by texture and color. Extrapolation of the linear part of the curve in Figure 11 to 1 cm shows that there should be several thousand xenoliths in the data set between 4 cm and 1 cm in eigenlength, if the xenolith population follows the fractal distribution down to that size. Thus, xenoliths of this size range are underrepresented, possibly due to dissolution or disaggregation (e.g., Farris and Paterson, 2007). Figure 18 shows a sphere simulation; spheres were generated with D_3 = 2.5 and were then decreased in radius by a constant value in order to simulate a constant linear rate of melting. Such a process preferentially affects the smaller particles, leading to a left-hand tailing off of the distribution.

Farris and Paterson (2007) studied xenolith size distributions in two Alaskan plutons using outcrop measurements and image analysis, and derived large D_2 values with a mean of 2.3 (Fig. 1). They reasoned that the 2D nature of their measurements does not affect the fractal dimension because random cuts through spheres generally result in an intersection diameter that is a large fraction of the true diameter (McCammon, 1975). This reasoning is faulty for reasons outlined above (e.g., Fig. 2). It is

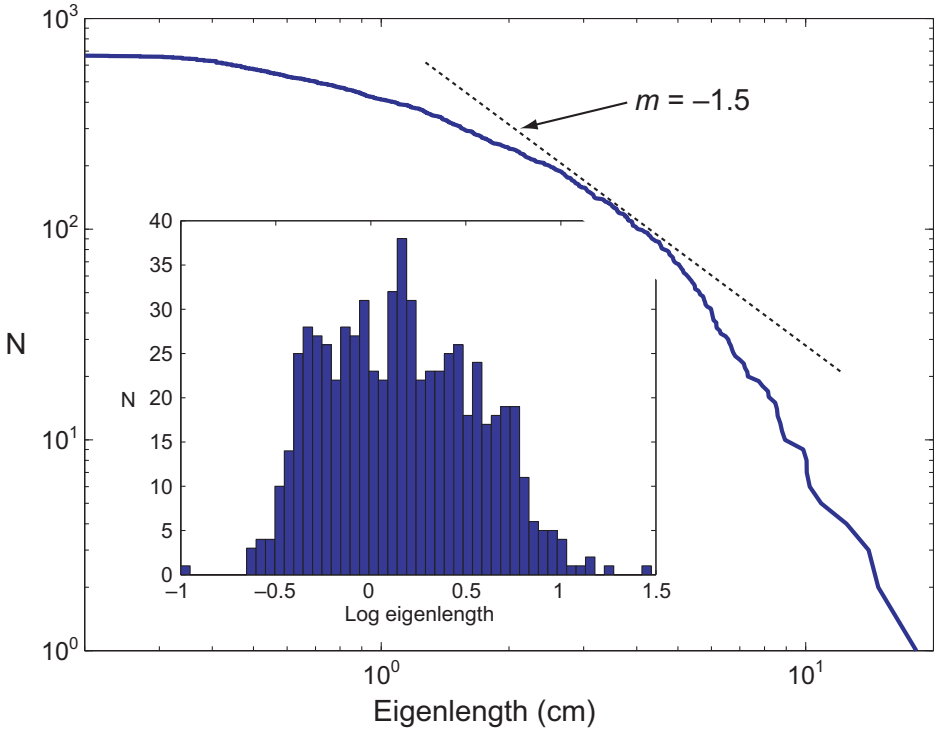

Figure 15. Size-distribution plot of Titus Canyon breccia. As with the crushed calcite, this array lacks a linear section, probably as a result of fragmentation via through-going fractures. *m*—slope of line segment.

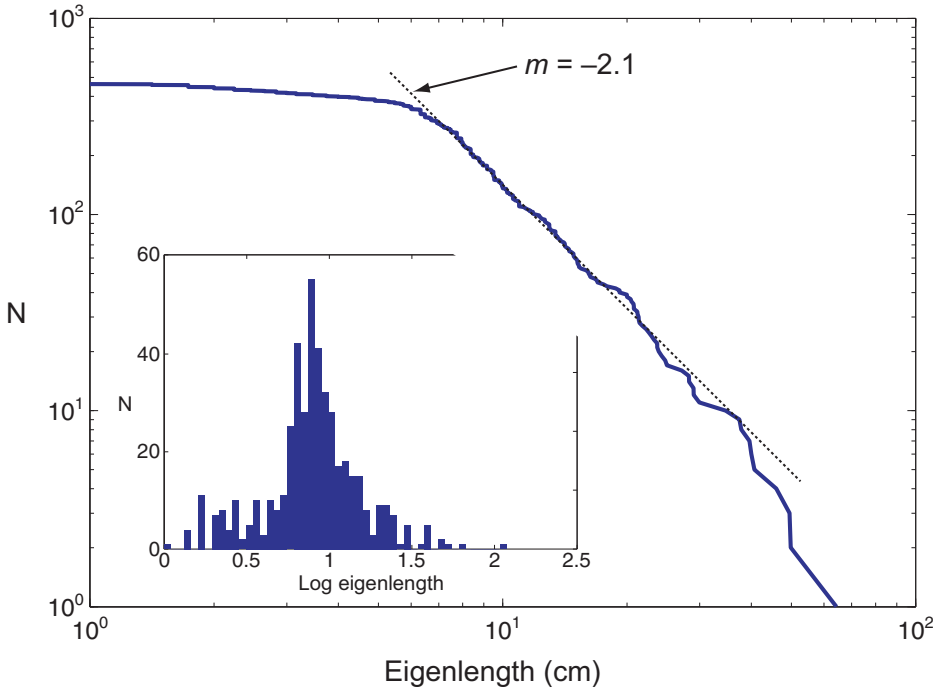

Figure 16. Size-distribution plot of 463 mafic enclaves in the Half Dome Granodiorite. These data suggest D_2 = 2.1, a high value consistent with other studies on enclaves (e.g., Perugini et al., 2007). *m*—slope of line segment.

not clear why their estimated D_2 values, which imply $D_3 > 3$ for four out of six measurements, are so high. For one pluton (Shaft Peak), the high number may be a result of the image analysis method used. Thresholding grayscale images is highly subjective unless the contrast between particles and background is high, as in Figure 8, and their example thresholded image (their fig. 10) appears to have broken many gray xenoliths into myriad tiny fragments. This would lead to an overestimate of *D*.

The size distribution of mafic enclaves we analyzed is consistent with the hypothesis that dispersal of mafic magma into felsic magma is a fractal process, but only over a restricted size range (Holtz et al., 2004; Perugini et al., 2007). Holtz et al. (2004) found $D_2 = 1.8$, whereas Perugini et al. (2007) derived D_2 ~2.5. This value implies a D_3 of 3.5, significantly higher than the fragmentation processes discussed above. The high D_2 values derived from our study (2.1) and by Perugini et al. (2007) indicate that there is a distinct difference between this process and the breakup of solid objects. The sharp decrease in enclave abundance at eigenlengths less than 6 cm is real; as with the xenolith study, enclaves were measured by close inspection of polished surfaces. In our study, nearly all measured enclaves have eigenlengths <50 cm, and the maximum measured eigenlength was ~2 m, consistent with the Sierra Nevada Range as a whole (Pabst, 1928; Tobisch et al., 1997; Barbarin, 2005). This size distribution is comparable to the distribution of the injections that comprise individual dikes in the Jurassic Independence dike swarm of eastern California (Glazner et al., 2008). In mafic dike swarms worldwide, dikes thinner than ~10 cm are rarely found (e.g., Jolly and Sanderson, 1995; Glazner et al., 2008), and well-exposed dikes are typically found to be highly composite. We speculate that if mafic enclaves form by disaggregation of mafic dikes into drops (e.g., Vernon, 1984; Barbarin, 2005), then their size distribution has upper and lower limits that are controlled by the aperture of the dikes that form them. Alternatively, the lower size limit may result from recrystallization and reaction with the surrounding granodiorite, making smaller enclaves hard to recognize.

CONCLUSIONS

Numerical simulations and physical fragmentation experiments demonstrate that the fractal dimension of an array of particles with fractal dimension *D* is generally $D - 1$ in a two-dimensional cut. This results in a size distribution in outcrop or thin section that is highly skewed compared to the true 3D array. However, in systems where there is a persistent set of fractures,

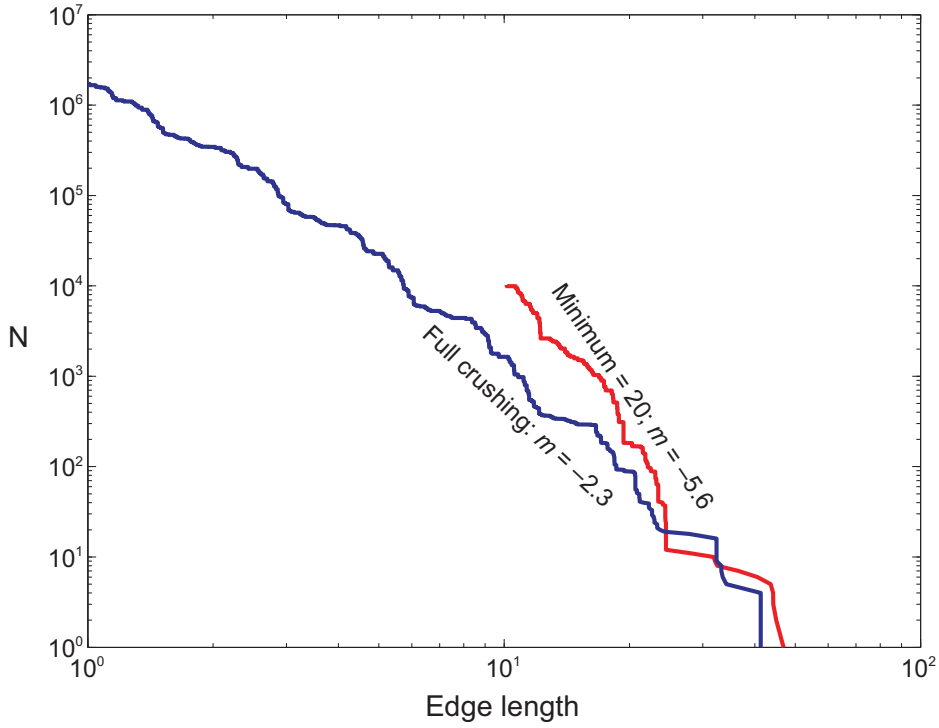

Figure 17. Particle arrays produced by randomly splitting cubes into eight sub-cubes, a self-similar process (see text for algorithm); seeded by 100 cubes drawn from *U*[1,100] (arbitrary units). Blue curve was produced by continuing this process for eight iterations. Red curve was produced by another simulation in which the minimum cube that can be split has edge length 20, to simulate a comminution limit. This curve is rotated clockwise from the first and has a much steeper slope, similar to the relationships in Figure 10. *m*—slope of line segment.

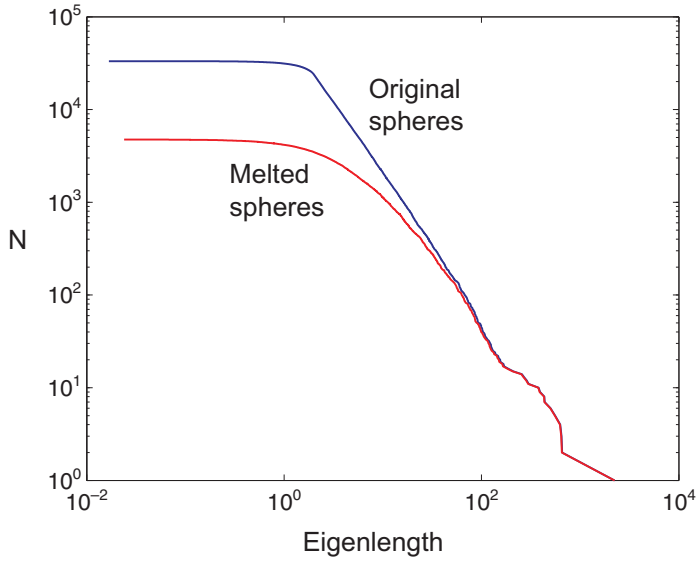

Figure 18. Simulation of a cut through an array of 10^6 spheres, as in Figure 4, with and without simulated loss of smaller particles by melting or disaggregation. Each sphere generated with *D* = 2.5 was decreased in radius by 2 units. Approximately 82% of all original spheres had a radius of 2 or fewer units and disappeared. The remaining spheres were cut by a plane as before. The resulting array on the size distribution plot is significantly rounded at the small end, falling below the *D* = 1.5 line; such a process could account for the relative lack of small xenoliths at May Lake.

such as a crystal with good cleavage or a well-fractured rock, the resulting particle arrays are continuously curved on a size-distribution plot, and lack the small particles predicted by a fractal distribution. Natural examples of fragmentation always lack the infinite number of particles predicted by a true fractal array but are commonly linear, with D_2 ~1.5 (corresponding to D_3 ~2.5) over an order of magnitude or more. Extensively fragmented rocks and minerals typically reach a comminution limit on the order of 1 µm, below which further brittle fracture is mechanically unfavorable. The range of lengths covered by observations of natural phenomena is typically limited to a few orders of magnitude. Observations are constrained on the small end of the scale by limitations of optical techniques of observation and sample handling problems, and on the large end of the scale by sampling issues and truncation of large objects by the boundary of the observation area.

ACKNOWLEDGMENTS

This work was supported by grants from the National Science Foundation to AFG (EAR-8816941, 8917291, 0336070, and 0538129). Chris Glazner helped with mathematical development. Data presented in this paper were collected over the course of several years, with the assistance of John Bartley, Drew Coleman, Kjell Lindgren, Bryan Law, Sam Coleman, Scott Hetzler, and Cecil Patrick, among many others. We thank Associate Editor Michael Cheadle for both an excellent review and efficient editorial handling, and two anonymous reviewers for helpful comments.

REFERENCES CITED

Allègre, C.J., Le Mouel, J.L., and Provost, A., 1982, Scaling rules in rock fracture and possible implications for earthquake prediction: Nature, v. 297, p. 47–49, doi:10.1038/297047a0.

Bagde, M.N., Raina, A.K., Chakraborty, A.K., and Jethwa, J.L., 2002, Rock mass characterization by fractal dimension: Engineering Geology, v. 63, p. 141–155, doi:10.1016/S0013-7952(01)00078-3.

Balme, M.R., Rocchi, V., Jones, C., Sammonds, P.R., Meredith, P.G., and Boon, S., 2004, Fracture toughness measurements on igneous rocks using a high-pressure, high-temperature rock fracture mechanics cell: Journal of Volcanology and Geothermal Research, v. 132, p. 159–172, doi:10.1016/S0377-0273(03)00343-3.

Barbarin, B., 2005, Mafic magmatic enclaves and mafic rocks associated with some granitoids of the central Sierra Nevada batholith, California: Nature, origin, and relations with the hosts: Lithos, v. 80, p. 155–177, doi:10.1016/j.lithos.2004.05.010.

Bateman, P.C., Kistler, R.W., Peck, D.L., and Busacca, A.J., 1983, Geologic map of the Tuolumne Meadows Quadrangle, Yosemite National Park, California: U.S. Geological Survey Map GQ-1570, scale 1:62,500.

Billi, A., 2005, Grain size distribution and thickness of breccia and gouge zones from thin (<1 m) strike-slip fault cores in limestone: Journal of Structural Geology, v. 27, no. 10, p. 1823–1837, doi:10.1016/j.jsg.2005.05.013.

Billi, A., and Storti, F., 2004, Fractal distribution of particle size in carbonate cataclastic rocks from the core of a regional strike-slip fault zone: Tectonophysics, v. 384, no. 1–4, p. 115–128, doi:10.1016/j.tecto.2004.03.015.

Boggs, S., 1992, Petrology of Sedimentary Rocks: New York, Macmillan, 707 p.

Broz, M.E., Cook, R.F., and Whitney, D.L., 2006, Microhardness, toughness, and modulus of Mohs scale minerals: The American Mineralogist, v. 91, p. 135–142, doi:10.2138/am.2006.1844.

Chanudet, V., and Filella, M., 2008, Size and composition of inorganic colloids in a peri-alpine, glacial flour-rich lake: Geochimica et Cosmochimica Acta, v. 72, p. 1466–1479, doi:10.1016/j.gca.2008.01.002.

Chayes, F., 1950, On the bias of grain-size measurements made in thin section: The Journal of Geology, v. 58, p. 156–160, doi:10.1086/625716.

Crum, S.V., 1990, Fractal concepts applied to bench-blast fragmentation, *in* Hustrulid, W.A., and Johnson, G.A., eds., Rock Mechanics: Contributions and Challenges: Proceedings of the 31st U.S. Symposium, Colorado School of Mines, Golden, 18–20 June, 1990: Rotterdam, A.A. Balkema, p. 913–919.

deMartin, B., Hirth, G., and Evans, B., 2004, Experimental constraints on thermal cracking of peridotite at oceanic spreading centers, *in* German, C.R., Lin, J., and Parson, L.M., eds., Mid-Ocean Ridges: Hydrothermal Interactions between the Lithosphere and Oceans: Washington, D.C., Geophysical Monograph Series Volume 148, American Geophysical Union, p. 167–185.

Devroye, L., 1986, Non-uniform random variate generation: New York, Springer-Verlag, 843 p.

Farris, D.W., and Paterson, S.R., 2007, Contamination of silicic magmas and fractal fragmentation of xenoliths in Paleocene plutons on Kodiak Island, Alaska: Canadian Mineralogist, v. 45, no. 1, p. 107–129, doi:10.2113/gscanmin.45.1.107.

Folk, R.L., and Ward, W.C., 1957, Brazos River bar [Texas]: A study in the significance of grain size parameters: Journal of Sedimentary Research, v. 27, no. 1, p. 3–26.

Ghosh, A., Daemen, J.J.K., and van Zyl, D., 1990, Fractal-based approach to determine the effect of discontinuities on blast fragmentation, *in* Hustrulid, W.A., and Johnson, G.A., eds., Rock Mechanics: Contributions and Challenges: Proceedings of the 31st U.S. Symposium, Colorado School of Mines, Golden, 18–20 June, 1990: Rotterdam, A.A. Balkema, p. 905–912.

Gimenéz, D., Allmaras, R.R., Huggins, D.R., and Nater, E.A., 1998, Mass, surface and fragmentation fractal dimensions of soil fragments produced by tillage: Geoderma, v. 86, p. 261–278, doi:10.1016/S0016-7061(98)00043-3.

Glazner, A.F., and Bartley, J.M., 1990, Early Miocene dome emplacement, diking, and limited tectonism in the northern Marble Mountains, eastern Mojave Desert, California, *in* Foster, J.F., and Lewis, L.L., eds., Lower Colorado River Extensional Terrane and Whipple Mountains Guidebook, Volume 18: Santa Ana, South Coast Geological Society, p. 89–97.

Glazner, A.F., and Bartley, J.M., 2006, Is stoping a volumetrically significant pluton emplacement process?: Geological Society of America Bulletin, v. 118, p. 1185–1195, doi:10.1130/B25738.1.

Glazner, A.F., Farmer, G.L., Hughes, W.T., Wooden, J.L., and Pickthorn, W., 1991, Contamination of basaltic magma by mafic crust at Amboy and Pisgah craters, Mojave Desert, California: Journal of Geophysical Research, v. 96, p. 13,673–13,691, doi:10.1029/91JB00175.

Glazner, A.F., Bartley, J.M., Coleman, D.S., Gray, W., and Taylor, R.Z., 2004, Are plutons assembled over millions of years by amalgamation from small magma chambers?: GSA Today, v. 14, p. 4–11, doi:10.1130/1052-5173(2004)014<0004:APAOMO>2.0.CO;2.

Glazner, A.F., Carl, B.S., Coleman, D.S., Miller, J.S., and Bartley, J.M., 2008, Chemical variability and the composite nature of dikes from the Jurassic independence dike swarm, eastern California, *in* Wright, J.E., and Shervais, J.W., eds., Ophiolites, Arcs, and Batholiths: A Tribute to Cliff Hopson: Geological Society of America Special Paper 438, p. 455–480.

Gray, W., Glazner, A.F., Coleman, D.S., and Bartley, J.M., 2008, Long-term geochemical variability of the Late Cretaceous Tuolumne Intrusive Suite, central Sierra Nevada, California: The Geological Society of London, Special Publications, v. 304, p. 183–201, doi:10.1144/SP304.10.

Hagan, J.T., 1981, Impossibility of fragmenting small particles: Brittle-ductile transition: Journal of Materials Science, v. 16, p. 2909–2911, doi:10.1007/BF02402857.

Hartmann, W.K., 1969, Terrestrial, lunar, and interplanetary rock fragmentation: Icarus, v. 10, no. 2, p. 201–213, doi:10.1016/0019-1035(69)90022-0.

Hatch, T., and Choate, S.P., 1929, Statistical description of the size properties of nonuniform particulate substances: Journal of the Franklin Institute, v. 207, p. 369–387, doi:10.1016/S0016-0032(29)91451-4.

Higgins, M.D., 1994, Numerical modeling of crystal shapes in thin section: Estimation of crystal habit and true size: The American Mineralogist, v. 79, p. 113–119.

Higgins, M.D., 2000, Measurement of crystal size distributions: The American Mineralogist, v. 85, p. 1105.

Holtz, F., Lenné, S., Ventura, G., Vetere, F., and Wolf, P., 2004, Non-linear deformation and breakup of enclaves in a rhyolitic magma: A case study from Lipari Island (southern Italy): Geophysical Research Letters, v. 31, p. L24611, doi:10.1029/2004GL021590.

Jolly, R.J.H., and Sanderson, D.J., 1995, Variation in the form and distribution of dykes in the Mull swarm, Scotland: Journal of Structural Geology, v. 17, p. 1543, doi:10.1016/0191-8141(95)00046-G.

Kendall, K., 1978, The impossibility of comminuting small particles by compression: Nature, v. 272, p. 710–711, doi:10.1038/272710a0.

Krumbein, W.C., and Tisdel, F.W., 1940, Size distribution of source rocks of sediments: American Journal of Science, v. 238, no. 4, p. 296–305, doi:10.2475/ajs.238.4.296.

Kueppers, U., Perugini, D., and Dingwell, D.B., 2006, "Explosive energy" during volcanic eruptions from fractal analysis of pyroclasts: Earth and Planetary Science Letters, v. 248, no. 3–4, p. 800–807, doi:10.1016/j.epsl.2006.06.033.

Mandelbrot, B.B., 1983, The fractal geometry of nature: San Francisco, W.H. Freeman, 468 p.

Marone, C., and Scholz, C.H., 1989, Particle-size distribution and microstructures within simulated fault gouge: Journal of Structural Geology, v. 11, p. 799–814, doi:10.1016/0191-8141(89)90099-0.

McCammon, R.B., 1975, Statistics and probability, *in* McCammon, R.B., ed., Concepts in Geostatistics: New York, Springer-Verlag, p. 1–20.

Meibom, A., and Balslev, I., 1996, Composite power laws in shock fragmentation: Physical Review Letters, v. 76, no. 14, p. 2492, doi:10.1103/PhysRevLett.76.2492.

Mills, R.D., Glazner, A.F., and Coleman, D.S., 2009, Scale of pluton/wall-rock interaction near May Lake, Yosemite National Park, California, USA: Contributions to Mineralogy and Petrology, v. 158, p. 263–281, doi:10.1007/s00410-009-0381-x.

Norris, R.M., 1985, A geologic guide to Titus Canyon, Death Valley National Monument, Inyo County: California Geology, v. 39, p. 195–202.

Pabst, A., 1928, Observations on inclusions in the granitic rocks of the Sierra Nevada: Bulletin Department of Geological Science, University of California, v. 17, p. 325–386.

Pepe, S., Solaro, G., Ricciardi, G.P., and Tizzani, P., 2008, On the fractal dimension of the fallout deposits: A case study of the 79 A.D. Plinian eruption at Mount Vesuvius: Journal of Volcanology and Geothermal Research, v. 177, no. 1, p. 288–299, doi:10.1016/j.jvolgeores.2008.01.023.

Perfect, E., 1997, Fractal models for the fragmentation of rocks and soils: A review: Engineering Geology, v. 48, p. 185–198, doi:10.1016/S0013-7952(97)00040-9.

Perugini, D., Valentini, L., and Poli, G., 2007, Insights into magma chamber processes from the analysis of size distribution of enclaves in lava flows: A case study from Vulcano Island (southern Italy): Journal of Volcanology and Geothermal Research, v. 166, p. 193–203, doi:10.1016/j.jvolgeores.2007.07.017.

Perugini, D., Speziali, A., Caricchi, L., and Kueppers, U., 2011, Application of fractal fragmentation theory to natural pyroclastic deposits; Insights into volcanic explosivity of the Valentano scoria cone (Italy): Journal of Volcanology and Geothermal Research, v. 202, p. 200–210, doi:10.1016/j.jvolgeores.2011.02.008.

Peterson, T.D., 1996, A refined technique for measuring crystal size distributions in thin section: Contributions to Mineralogy and Petrology, v. 124, p. 395–405, doi:10.1007/s004100050199.

Pickering, G., Bull, J.M., and Sanderson, D.J., 1995, Sampling power-law distributions: Tectonophysics, v. 248, p. 1–20, doi:10.1016/0040-1951(95)00030-Q.

Rogers, J.J.W., 1965, Reproducibility and significance of measurements of sedimentary size distributions: Journal of Sedimentary Petrology, v. 35, no. 3, p. 722–732.

Rose, R.L., 1957, Geology of the May Lake area, Yosemite National Park: Berkeley, California, University of California, Berkeley, 224 p.

Rosenbaum, J.G., and Reynolds, R.L., 2004, Record of Late Pleistocene glaciation and deglaciation in the southern Cascade Range: II. Flux of glacial flour in a sediment core from Upper Klamath Lake, Oregon: Journal of Paleolimnology, v. 31, p. 235–252, doi:10.1023/B:JOPL.0000019229.75336.7a.

Rousell, D.H., Fedorowich, J.S., and Dressler, B.O., 2003, Sudbury Breccia (Canada): A product of the 1850 Ma Sudbury event and host to footwall Cu-Ni-PGE deposits: Earth-Science Reviews, v. 60, p. 147–174, doi:10.1016/S0012-8252(02)00091-0.

Russ, J.C., 1994, Fractal Surfaces: New York, Plenum Press, 309 p.

Sahagian, D.L., and Proussevitch, A.A., 1998, 3D particle size distributions from 2D observations: Stereology for natural applications: Journal of Volcanology and Geothermal Research, v. 84, no. 3–4, p. 173–196, doi:10.1016/S0377-0273(98)00043-2.

Sammis, C., King, G., and Biegel, R., 1987, The kinematics of gouge deformation: Pure and Applied Geophysics, v. 125, no. 5, p. 777–812, doi:10.1007/BF00878033.

Shimamoto, T., and Nagahama, H., 1992, An argument against the crush origin of pseudotachylytes based on the analysis of clast-size distribution: Journal of Structural Geology, v. 14, p. 999–1006, doi:10.1016/0191-8141(92)90031-Q.

Snow, J.K., Wernicke, B.P., Burchfiel, B.C., Hodges, K.V., Axen, G.J., Walker, J.D., and Guth, P.L., 1989, Extensional tectonics in the Basin and Range Province between the southern Sierra Nevada and the Colorado Plateau: Washington, D.C., International Geological Congress Field Trip Guidebook T138, American Geophysical Union, 80 p.

Suzuki-Kamata, K., Kusano, T., and Yamasaki, K., 2009, Fractal analysis of the fracture strength of lava dome material based on the grain size distribution of block-and-ash flow deposits at Unzen Volcano, Japan: Sedimentary Geology, v. 220, p. 162–168, doi:10.1016/j.sedgeo.2009.04.026.

Tang, D., and Marangoni, A.G., 2006, 3D fractal dimension of fat crystal networks: Chemical Physics Letters, v. 433, p. 248–252, doi:10.1016/j.cplett.2006.11.057.

Tavassoli, Z., and Shirvani, A. E., 2000, Models of fragmentation with power law log-normal distributions: Physica A: Statistical Mechanics and Its Applications, v. 286, no. 1–2, p. 29–44.

Taylor, R.Z., 2004, Structure and stratigraphy of the May Lake interpluton screen, Yosemite National Park, California [M.S. thesis]: University of North Carolina, 61 p.

Tobisch, O.T., McNulty, B.A., and Vernon, R.H., 1997, Microgranitoid enclave swarms in granitic plutons, central Sierra Nevada, California: Lithos, v. 40, p. 321–339, doi:10.1016/S0024-4937(97)00004-2.

Turcotte, D.L., 1986, Fractals and fragmentation: Journal of Geophysical Research, v. 91, p. 1921–1926, doi:10.1029/JB091iB02p01921.

Turcotte, D.L., 1989, Fractals in geology and geophysics: Pure and Applied Geophysics, v. 131, p. 171–196, doi:10.1007/BF00874486.

Vernon, R.H., 1984, Microgranitoid enclaves in granites: Globules of hybrid magma quenched in a plutonic environment: Nature, v. 309, p. 438–439, doi:10.1038/309438a0.

Yazdi, M., and Esmaeilnia, A., 2009, Natural fragmentation model of Zirab coals, Iran: The Open: Geological Journal, v. 3, p. 1–7.